Unstable blast shocks in dilute granular flows

Jean-François Boudet, Hamid Kellay

Unstable blast shocks in dilute granular flows

J. F. Boudet and H. Kellay
U. Bordeaux 1, Laboratoire Ondes et Matière d'Aquitaine (UMR CNRS 5798), 351 cours de la Libération, 33405 Talence, France
(Received 3 May 2012; published 7 May 2013)

Shocks and blasts can be readily obtained in granular flows be they dense or dilute. Here, by examining the propagation of a blast shock in a dilute granular flow, we show that such a front is unstable with respect to transverse variations of the density of grains. This instability has a well-defined wavelength which depends on the density of the medium and has an amplitude which grows as an exponential of the distance traveled. These features can be understood using a simple model for the shock front, including dissipation which is inherent to granular flows. While this instability bears much resemblance to that anticipated in gases, it is distinct and has special features we discuss here.

DOI: 10.1103/PhysRevE.87.052202 PACS number(s): 45.70.Mg, 47.40.−x

I. INTRODUCTION

Granular media can be subjected to strong-enough solicitations to produce shocks in dense [1–3] as well as dilute [4–7] materials and blastlike perturbations in the dilute gaseous limit [8,9]. In gases, a blast shock ensues when a large amount of energy is deposited during a short time in a small spatial extent. The blast or explosion then expands as a thin shell at speeds much higher than the speed of sound in the surrounding medium. This problem has received much attention, starting with the work of Taylor and the work of Sedov, who predicted, independently from each other, the temporal evolution of the blast radius versus time in the case of energy conserving blasts [10,11]. The instability of such fronts has been studied since the 1960s with ongoing work as of the present date [12–14]. Several issues have to be examined such as the nature of the surrounding gas, the presence or not of different dissipation mechanisms as may happen in the presence of radiative processes, for example, and the exact details of the shell as well as the geometry of the blast [15–18]. The question of the stability of such blasts has haunted specialists in diverse fields for more than half a century. To realize the importance of this question consider a supernova or other interstellar explosion. If such explosions become unstable, the front will spread matter in clumps. These considerations are important for the distribution of matter in the universe and the ensuing formation of clusters giving birth to stars or other interstellar objects [17–19].

As mentioned above, recent work has shown that dilute granular flows may be used to understand the structure of shock waves and the dynamics of blasts [4–9,20]. Besides the advantage that blast propagation can be captured with relative ease in granular flows, this system has the additional feature of possessing inelastic collisions so the role of dissipation can be gauged precisely. The question we ask here concerns the stability of such blasts.

Here, and by using a granular gas as a model system, we show that linear blast shocks can be unstable. This instability can be understood in an analogous way as for blasts in gases [13,14,21] but with important modifications notably dissipation due to inelastic collisions between grains [22]. The most important result is that the wavelength of maximum growth is determined by the mean free path of the gas and that the growth rate is proportional to the velocity of the blast. These two results can be obtained from a theoretical analysis of the dynamics of small perturbations added to the blast front modeled as a simple step of density and velocity.

II. FRONT PRODUCTION AND PROPAGATION

We produced linear blasts propagating down an inclined plane using a simple experimental setup shown in the schematic of Fig. 1. The experiments used glass beads, of different diameters d ranging from 100 to 500 μm, released from a reservoir (equipped with a gate of variable height) as a thin and dilute sheet flowing down the plane made of 4-mm-thick glass. The opening height of the gate controls the density Φ_0 of the grains in the thin sheet which is estimated from the flux of grains, a measurement of the stream velocity, and a measurement of the thickness of the layer. This sheet of grains accelerates down the plane after its exit from the reservoir. The velocity of the flow, U_{flow} as well as its fluctuations are determined using particle tracking of individual grains or grain aggregates. Velocity fluctuations arise most probably from collisions between grains as well as through the entrance conditions. A long and thin rod is used to produce linear blast shocks which propagate in the direction of the main flow. The velocity of the flow at the chosen location for producing the blast is 1 m/s and the area examined is about 10 cm in length and about 15 cm in width. The variation of the velocity in this area is roughly 10%. In previous work [8], we had shown that the impact of a small sphere on such a dilute flow produces small holes almost devoid of grains and whose diameter increases in time in a manner analogous to that of circular blasts in gases. In the case described here, the impact of the rod onto the flow produces a strip devoid of grains whose width increases in time. The origin of elapsed time is taken to be the moment when the strip rod hits the thin sheet of grains. The rod has an impact time of about 0.2 ms and an impact velocity of about 10 m/s. The strip formed by the impact of the rod is delimited by two fronts that are more dense than the flowing granular medium and which propagate in opposite directions with respect to the center of the strip. This process is filmed with a fast camera to follow the evolution of the strip as it is advected downstream from the impact zone by the mean flow of the dilute granular sheet. The rod actually rebounds on the glass plate so it does not interfere with the future propagation of the strip. The images

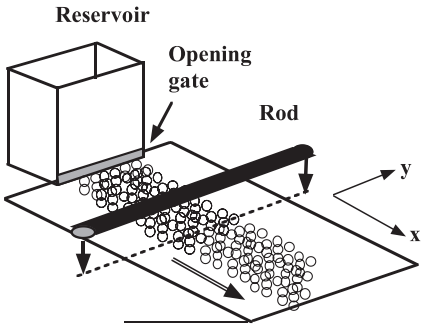

FIG. 1. Schematic of the setup: The glass beads are released from a reservoir (equipped with a gate of variable height) as a thin and dilute sheet flowing down the plane made of 4-mm-thick glass. The opening height of the gate controls the density of the grains in the thin sheet, which accelerates down the plane after its exit from the reservoir. A long and thin rod is used to produce linear blast shocks propagating in the direction of the main flow.

in Fig. 2 give an illustration of the opening of the strip almost devoid of grains and the ensuing propagation of upstream and downstream propagating fronts. Figure 2(b) shows an average intensity profile in the direction of propagation. The interior region (where the rod impacted) is almost devoid of grains, as the rod displaced them towards the thicker fronts and appears as white in the photographs. This region has been used as a reference and its intensity has been set to zero to indicate zero grain density. The darker regions representing the blast fronts appear as two maxima separated by a distance $2R$, the width of the blast. Their intensity is indicative of a higher density than the surroundings. Farther away from these two maxima, the intensity decreases to a constant level to indicate the density of the outer medium. In Fig. 3(a), the separation $2R$ between the upstream and downstream fronts is plotted versus time. This separation increases fast at first, before increasing linearly versus time at the later stages as indicated by the dashed lines. The initial increase has a large velocity which decreases continuously with time of propagation as shown in Fig. 3(b) before settling on a roughly constant velocity at the later instants in the linear region for $R(t)$. These features are representative of blast propagation with the last instants characterized by a velocity near that of the speed of sound in the material, about 10 cm/s, and initial instants with supersonic speeds [8]. From our experimental results, the velocity of the front in the blast regime follows

$$U(t) = \frac{dR(t)}{dt} = U_0 \exp\left[-\frac{R(t)}{L}\right] \tag{1}$$

or, equivalently,

$$R(t) = L \ln(tU_0/L + 1), \tag{2}$$

where L is a characteristic length scale. Figues 3(a) and 3(b) show fits to these functional forms. This variation differs from that of blasts in gases where power-law growth is found [10,11].

III. INSTABILITY OF THE FRONT: WAVELENGTH AND GROWTH RATE

As noted above, a dense region separates the region devoid of grains from the granular gas region. We will focus on the shock front separating this dense region from the granular gas

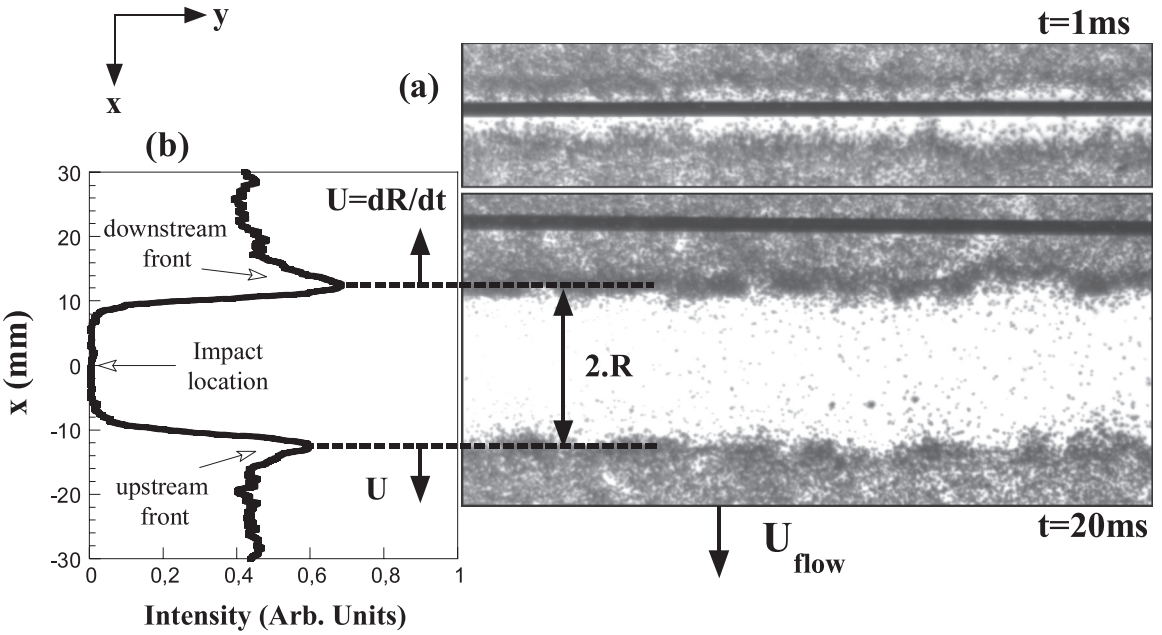

FIG. 2. (a) Formation of the blast at different instants after impact. The dark line in the middle is the rod. Once the rod impacts the flow, a strip devoid of grains forms. This strip is delimited by two denser regions we call the fronts. Both fronts are advected by the mean flow at a velocity U_{flow}. Each front travels at a relative velocity U with respect to the center of the strip as the width $2R$ of the strip increases in time. (b) Intensity profile in the direction perpendicular to the flow (using an inverted scale where white corresponds to zero grain density near the impact zone while black corresponds to a higher density). The two fronts appear as two well-defined peaks while the flowing granular medium appears with a lower density ($d = 0.33$ mm, $\Phi_0 = 0.05$, $\lambda = 11$ mm).

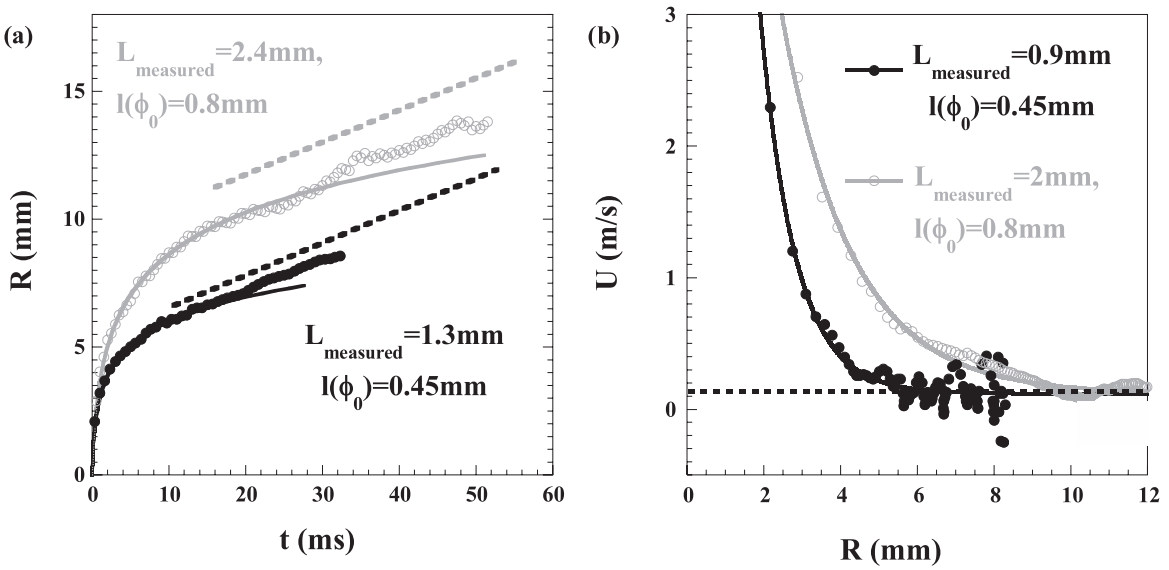

FIG. 3. (a) R versus time for different volume fractions (circles: $d = 0.33$ mm, $\Phi_0 = 0.05$; dots: $d = 0.33$ mm, $\Phi_0 = 0.09$). A fit using the functional form given in Eq. (2) is shown. The parameters of the fit are given in the figure. The dashed lines indicate the constant velocity regime at the end of the blast regime. (b) Velocity versus R, and a test of the functional form of the velocity versus R [Eq. (1)]. The parameters of the fit are given in the figure. Here the conditions are the same as described for panel (a) (circles: $d = 0.33$ mm, $\Phi_0 = 0.05$, dots: $d = 0.33$ mm, $\Phi_0 = 0.09$).

region. Note that this front is not homogeneous and develops an instability in the transverse direction to the flow with a roughly well-defined wavelength as shown in Fig. 4(a). Despite the low contrast between the dense and less dense regions along the front, the averaged intensity (which is indicative of the density of grains), shown in Fig. 4(a) below the photographs of the front, clearly shows that while the density is inhomogeneous right after impact, it becomes modulated in the direction parallel to the front. A sinusoidal variation is plotted on the intensity variation as a guide to the eye. From such analyses, an average wavelength can be obtained by measuring the average distance between intensity peaks. While most of our analyses focus on the upstream propagating front since the downstream front is usually hidden by the rod creating the blast, the main wavelength measured on the two fronts seems comparable. Additional measurements of the wavelength were carried out using Fourier analysis of the images. A typical spectrum is shown in Fig. 4(b). The position of the peak gives a measurement of the wavelength of the modulation in agreement with the wavelgnth determined from an average distance between intensity peaks. This instability actually grows in amplitude as it propagates, as illustrated by the snapshots of the front taken at different times after the impact of the rod and by the intensity profiles in Fig. 4(a). The blast is,

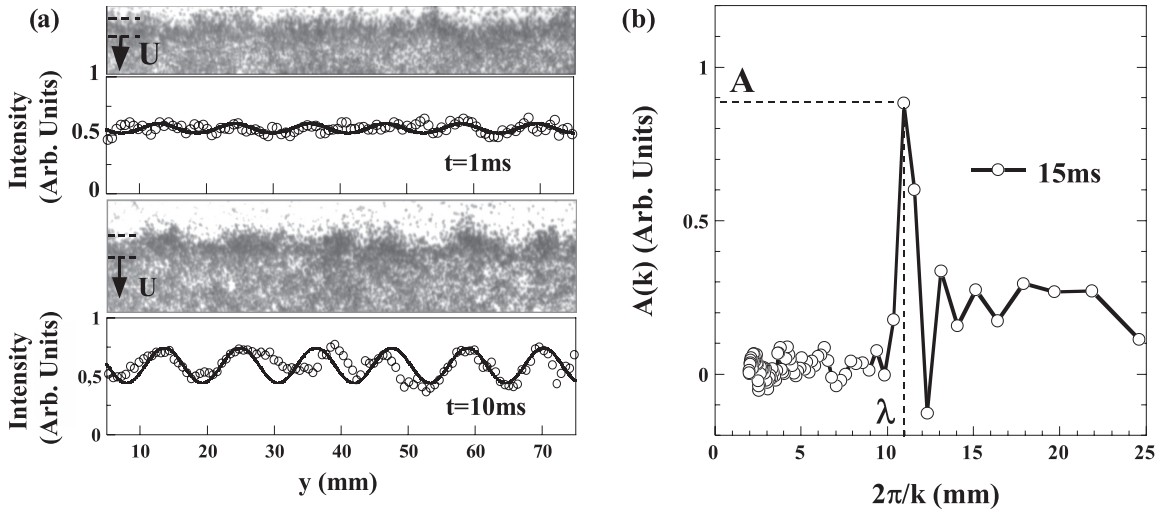

FIG. 4. (a) Upstream front at two different instants along with an intensity profile in the transverse direction ($d = 0.33$ mm, $\Phi_0 = 0.05$, $\lambda = 11$ mm). The intensity was averaged over the width of the front indicated by the two dashed lines. Note that 1 ms after impact, the density modulation is barely visible in the intensity signal while, at a later time ($t = 10$ ms), the modulation is clearly visible with the intensity profile showing a clear modulation and a well-defined wavelength. Sinusoidal modulation was added as a guide to the eye. (b) Fourier transforms of the second image in (a). Note that a well-defined peak is clearly observed at a similar wavelength as that deduced from the image.

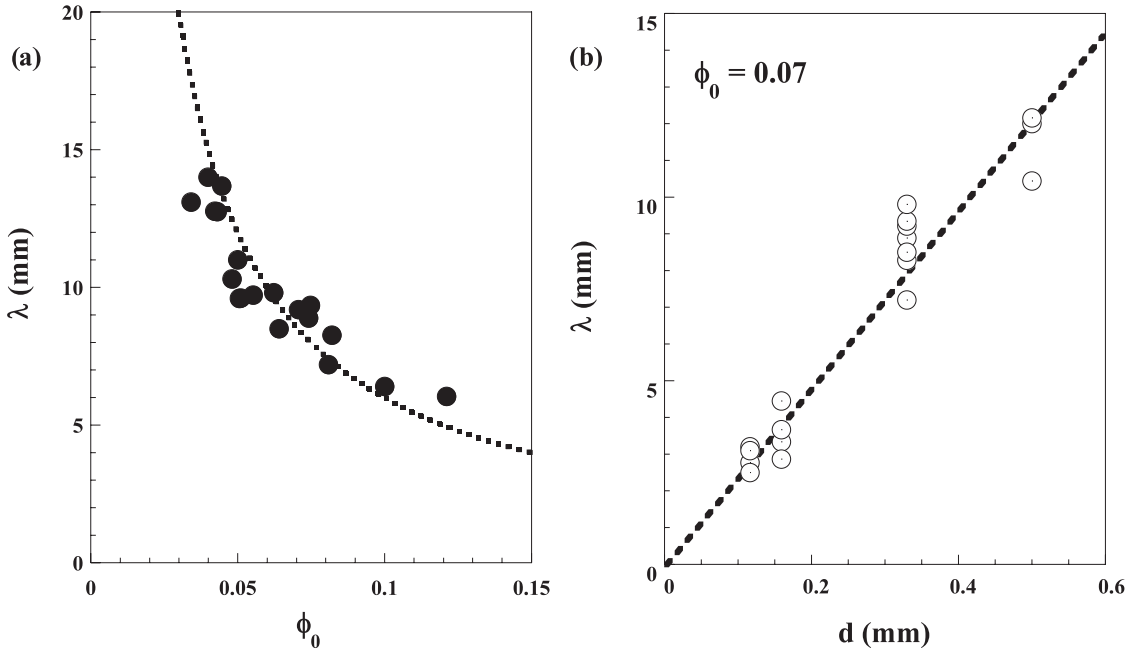

FIG. 5. (a) Characteristic wavelength of the instability for different incident volume fractions for $d = 0.33$ mm and (b) the wavelength versus grain diameter for a fixed volume fraction.

thus, unstable. The wavelength appears to be roughly constant with time of evolution but depends on the grain size and on the density of the flowing granular gas. This is illustrated in Figs. 5(a) and 5(b), which show that the wavelength which is of order 1 cm for the most dilute flows decreases with the density down to a few mm. Higher densities were much more difficult to analyze as the wavelength becomes comparable to the width of the front. This wavelength also increases roughly linearly with grain diameter, for a fixed volume fraction, as shown in Fig. 5(b).

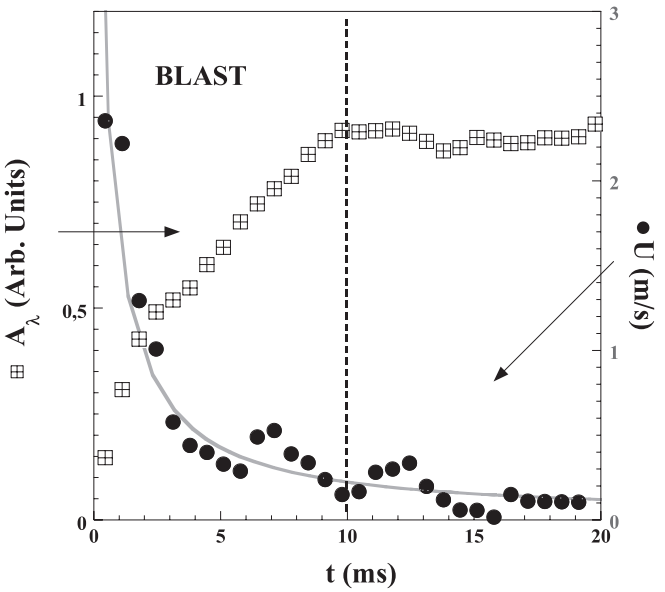

FIG. 6. Amplitude of the modulation (squares) versus time extracted from a Fourier analysis of the front ($d = 0.33$ mm, $\Phi_0 = 0.05$, $\lambda = 11$ mm). The velocity of the front (dots) versus time is also shown.

The second observation concerns the growth of the instability of the front. By analyzing the evolution of the front, we obtain the amplitude of this modulation versus time using Fourier analysis as in Fig. 4(b). The Fourier spectra show a well-defined peak at a well-defined wavelength. The amplitude A_λ of this peak is then followed versus time. The peak amplitude, shown in Fig. 6(a), starts out small and increases as time increases. This amplitude then saturates before starting to decrease. During the increase of the amplitude, the denser patches become more visible and better defined while during the last instants when the amplitude decreases, the patches become less visible and spread out. Along with the measurement of the amplitude of this mode, we show the velocity of the front in Fig. 6(a). Note that the amplitude of the observed perturbation increases only when the blast is supersonic. When the blast moves at the speed of sound, the perturbation stops growing. It turns out that $A_\lambda(t)$ grows exponentially versus $R(t)$ in the blast regime as shown in Fig. 7(a),

$$A_\lambda(t) = A_0 \exp\left[\frac{R(t)}{L'}\right], \tag{3}$$

where L' is a characteristic length. This functional form differs from those encountered in classical hydrodynamic instabilities (exponential growth versus time) and in the blast instability in gases (power-law growth in time). This functional form for A_λ implies that the growth rate is as follows:

$$w(t) = \frac{1}{A_\lambda(t)}\frac{dA_\lambda}{dt} = \frac{1}{L'}U. \tag{4}$$

The sign of $1/L'$ and its amplitude determine whether the instability grows and how fast it grows. This relation is verified

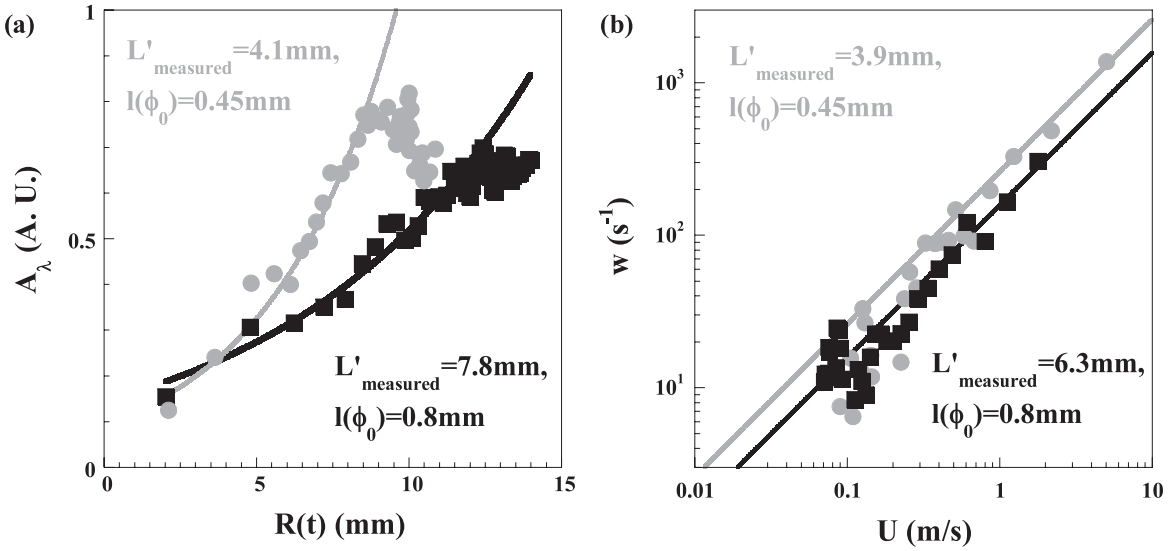

FIG. 7. (a) Amplitude of the perturbation versus R (dots: $d = 0.33$ mm, $\Phi_0 = 0.05$; squares: $d = 0.33$ mm, $\Phi_0 = 0.09$). The lines are fits using the functional form given in Eq. (3) in the text. The parameters of the fit are given. (b) Variation of the growth rate [Eq. (4)] versus the velocity of the front for the same data as in (a) (the same symbols are used).

experimentally as shown in Fig. 7(b), allowing for a direct measurement of L', which is clearly positive.

IV. ANALYSIS OF THE INSTABILITY

In order to understand the observed instability which we recall is analogous to the blast instability in gases [13,14], we recast the description of the instability for the case of a granular material since dissipation must play a dominant role in our case. As the flowing sheet is very thin (a few grain diameters thick), we describe the flow as two dimensional and use mass and momentum conservation and the energy balance equation which we write, respectively, as

$$\frac{\partial \Phi}{\partial t} + \frac{\partial \Phi V_i}{\partial x_i} = 0, \tag{5}$$

$$\frac{\partial \Phi V_j}{\partial t} + \frac{\partial \Phi V_i V_j}{\partial x_i} = -\frac{\partial P}{\partial x_j}, \tag{6}$$

$$\frac{\partial \Phi E}{\partial t} + \frac{\partial}{\partial x_i}[(\Phi E + P)V_i] = \frac{\partial}{\partial xi}\left(\kappa \frac{\partial T}{\partial xi}\right) - \gamma. \tag{7}$$

Here i and j refer to the coordinates x and y parallel and perpendicular to the flow direction. The volume fraction is Φ, the granular temperature is T, the velocity is $\mathbf{V}$, and the pressure is $P = \Phi T$. The internal energy E is given by $\frac{3}{2}T + \frac{1}{2}\mathbf{V}^2$. The dissipation γ and the thermal conductivity term κ are [22]

$$\gamma = \beta(1 - e^2)\frac{\Phi}{l(\Phi)}T^{3/2}, \tag{8}$$

$$\kappa = \alpha l(\Phi)\Phi\sqrt{T}, \tag{9}$$

$$l(\Phi) = d/(6\sqrt{2}\Phi), \tag{10}$$

where $l(\Phi)$ is the mean free path in the material and the sole characteristic length scale of the problem. α and β are unknown constants and e the coefficient of restitution of the glass beads. The temperature T is taken as the square of the velocity fluctuations. For simplicity, we model the shock front as a step function of density of grains and velocity of the particles. We focus on the descending front propagating upstream into the dilute surrounding gas (see the schematic in Fig. 8). We use a simplified description whereby the front is delimited by a volume fraction Φ_0 on the dilute side (i.e., in the granular gas region upstream from the front) and a volume fraction Φ_1 on the dense part. We do not take into account the fact that the density of the front decreases to zero in the region where the impact occurred. The front is advancing at a velocity $U(t)$. In the high Mach number limit (which is the case here as $M \sim 10$, since the velocity of sound is near 10 cm/s while typical velocities of the front are of order 100 cm/s) [5,8], and in the simplest possible form, we can write the shock conditions as follows:

$$\Phi_1 = \frac{1}{a}\Phi_0, \tag{11}$$

$$T_1 = aU^2, \tag{12}$$

where T_1 is the granular temperature in the dense part and a is an unknown constant. We further assume that Φ_1 is

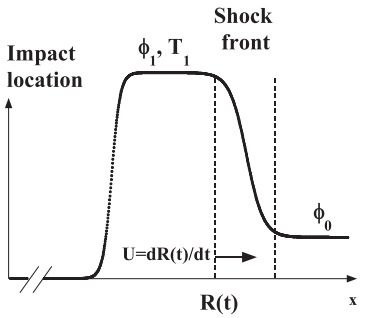

FIG. 8. Schematic of the shock front. The front is delimited by a volume fraction Φ_0 on the dilute side (i.e., in the granular gas region upstream from the front) and a volume fraction Φ_1 on the dense part. The front is advancing at a velocity $U(t)$.

independent of the position x along the flow direction and that all the particles in the dense front move with a velocity $V_x(t) = U(t)$.

From our experimental results, the velocity of the front follows $U(t) = U_0 \exp[-\frac{R(t)}{L}]$, as shown in Fig. 3. The length scale L, obtained from fitting such curves, turns out to be proportional to the mean free path: $L \sim 4l(\Phi_0)$. This functional form for U is compatible with the above equations. In the simplest possible case where the density, pressure, temperature, and velocity are constant and do not vary with x, and from $\partial(\Phi E)/\partial t = -\gamma$ and the shock conditions, we obtain $\frac{dV_x^2}{dt} \sim \frac{V_x^3}{l(\Phi_0)}$, giving $V_x(t) \sim \exp[-\frac{R(t)}{L}]$ with L proportional to the mean free path. While the resolution for L is complicated in the more realistic case where the pressure and the temperature away from the front are not constant, it does, however, remain proportional to $l(\Phi_0)$.

We now focus on the evolution of a small perturbation of the front along the direction y. The base state, taken as independent of y, is written as

$$\Phi_1 = Cts, \tag{13}$$

$$T = T_1 + (dV_x/dt)[R(t) - x], \tag{14}$$

$$P = \Phi_1\{T_1 + (dV_x/dt)[R(t) - x)]\}, \tag{15}$$

and the velocity as $V_x(t) = U_0 \exp[-R(t)/L]$, with $L \sim l(\Phi_0)$. Here x is the longitudinal distance from the impact point to the front position $R(t)$. The dependence on x comes from Eqs. (5)–(7) stated above and brings forth the dependence of the temperature and the pressure on the distance to the front.

We then consider a small perturbation of the volume fraction along the y axis with waven umber k,

$$\Phi(y,t) = \Phi_1 + A(t)\exp(iky). \tag{16}$$

This leads to {from mass conservation [Eq. (5)] and momentum conservation [Eq. (6)]} a perturbation of the base state with perturbations given by

$$V_y = -\frac{A'}{ik\Phi_1}\exp(iky), \tag{17}$$

$$\delta T = -\frac{1}{\Phi_1}\left(\frac{A''}{k^2} + AT_1\right)\exp(iky), \tag{18}$$

$$\delta P = -\frac{A''}{k^2}\exp(iky). \tag{19}$$

The primes indicate time derivatives. The energy balance equation for $x = R(t)$, i.e., at the front position to simplify the analysis, leads to an evolution equation for the amplitude of the instability,

$$\frac{3}{2}\frac{A'''}{k^2} + BA'' + \frac{5}{2}A'T_1 + CA = 0, \tag{20}$$

$$B = \left[\frac{3\beta(1-e^2)}{2l(\Phi_1)}\frac{\sqrt{T_1}}{k^2} + \frac{\alpha l(\Phi_1)}{4k^2}\frac{(dV_x/dt)^2}{T_1^{3/2}} + \alpha l(\Phi_1)\sqrt{T_1}\right], \tag{21}$$

$$C = \left[\frac{\alpha l(\Phi_1)}{4}\frac{(dV_x/dt)^2}{T_1^{1/2}} + \alpha l(\Phi_1)T_1^{3/2}k^2 - \frac{\beta(1-e^2)}{2l(\Phi_1)}T_1^{3/2}\right]. \tag{22}$$

The form $A(t) = A_0\exp(R(t)/L')$ is a solution to Eq. (20) and is in excellent agreement with our experiments (see Fig. 7). By introducing the reduced variables [here $l(\Phi_1) = al(\Phi_0)$],

$$X = \frac{\alpha}{a^{3/2}}\frac{l(\Phi_1)}{L}, \tag{23}$$

$$Y = \frac{\alpha}{a^{3/2}}\frac{l(\Phi_1)}{L'}, \tag{24}$$

$$K = \frac{\alpha}{a^{1/2}}kl(\Phi_1), \tag{25}$$

$$\beta' = \frac{\alpha\beta(1-e^2)}{a}, \tag{26}$$

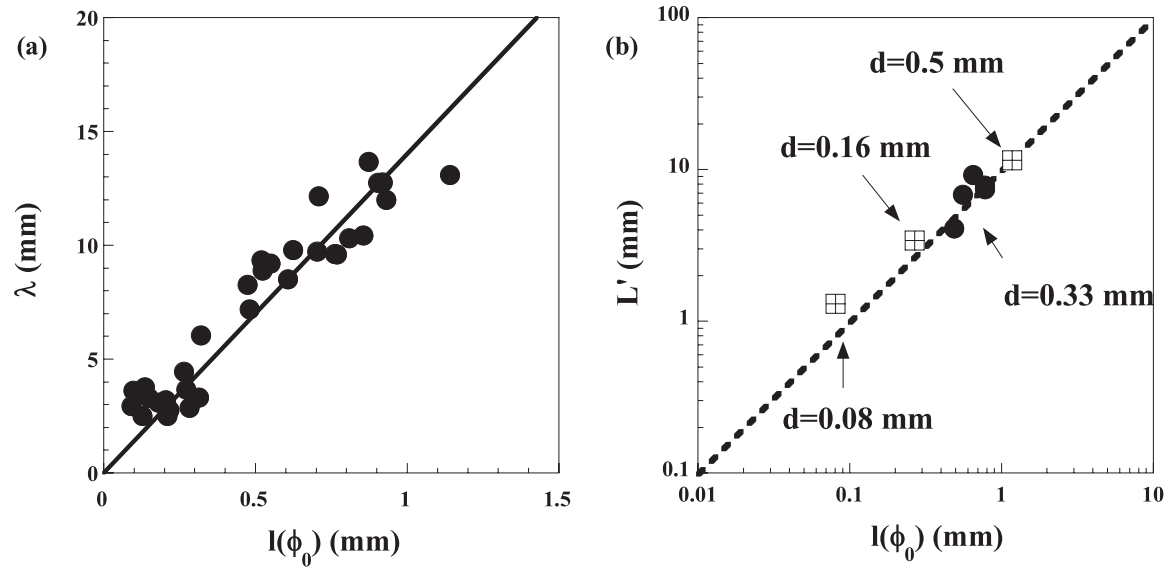

FIG. 9. (a) Wavelength and (b) characteristic length of the instability versus mean free path which was varied by using (crossed squares) different grains diameters (indicated near the data points) or a fixed diameter and different Φ_0 (dots).

we can rewrite Eq. (20) to obtain a nondimensional equation for L' versus k and, therefore, the growth of the instability for different wave numbers:

$$\frac{3a}{2K^2}Y(Y-X)(Y-2X)+aY(Y-X)B''+\frac{5}{2}Y+C''=0, \tag{27}$$

$$B''=\left(1+\frac{X^2}{4K^2}+\frac{3\beta'}{2K^2}\right), \tag{28}$$

$$C''=\left(K^2+\frac{X^2}{4}-\frac{\beta'}{2}\right). \tag{29}$$

This is a cubic equation which, in the limit of small K, and therefore small Y, can be approximated by a linear equation whose solution is

$$Y\sim\frac{\frac{\beta'}{2}-\frac{X^2}{4}}{aX\left(3X-\frac{X^2}{4}-\frac{3\beta'}{2}\right)}K^2. \tag{30}$$

For the instability to develop and grow, the prefactor in front of K^2 needs to be positive. Along with this condition, and since we observe a well-defined wavelength which we assume to be the wavelength of maximal growth, we impose that the dispersion relation goes through a maximum. These two conditions imply that the length scale L, which determines the deceleration of the front, needs to obey

$$\sqrt{\frac{\alpha}{2a^2\beta(1-e^2)}}l(\Phi_1)<L<\frac{2l(\Phi_1)}{a^{1/2}\beta(1-e^2)}. \tag{31}$$

Thus, the front needs to decelerate so dissipation needs to be important. However, this deceleration cannot occur over very short distances so the instability may have time to grow.

Figures 9(a) and 9(b) show the characteristics of the observed instability: the wavelength λ and the length L', from different runs using different volume fractions and different grain sizes, depend on a single parameter, the mean free path, in accordance with our analysis. The wavelength comes out to be $\lambda\sim 14l(\Phi_0)$ and the characteristic length turns out to be $L'\sim 10l(\Phi_0)$. These two parameters, λ and L', allow us to test the dispersion relation obtained from Eq. (27) and reported in Fig. 10 showing that the growth rate of the instability is positive for large wavelengths with a well-defined maximum. This feature is characteristic of classical hydrodynamic instabilities with bell-shaped dispersion relations. If we assume that the wavelength we observe is that of maximum growth (as it appears naturally in our experiments), the values of the predicted growth rates turn out to be consistent with our measurements as shown in Fig. 10. To mimic the dispersion relation we obtain experimentally, i.e., L' versus k, a choice of $\alpha=0.9$ and $\beta=0.7$ has been used. The value of a is estimated to be near 0.16 [23]. The range of allowed values for the dispersion relation to agree with our measurements turns out to be $0<\alpha<4$ and $\beta\sim 0.7$, in agreement with the condition above. A crucial ingredient of this instability is the presence of dissipation. Indeed, an increase of the local density of the front implies a decrease of the temperature due to an increase of the number of collisions. In the same way, this increase engenders a variation of the pressure. Since the modulation of the pressure decreases away from the front, it can become out of phase with the modulation in density. This implies that in the dilute regions of the front, both the pressure and the temperature can become larger than in the less dilute regions, giving rise to a nonzero flux of particles from the dilute regions to the more dense ones and, thus, reinforcing the instability.

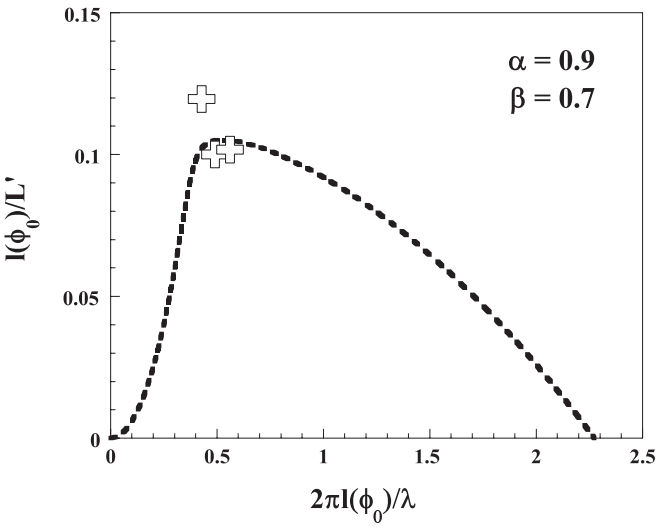

FIG. 10. Calculated dispersion relation [Eq. (27)] and estimates using the experimental values (the crossed squares) from Fig. 9(b).

V. CONCLUSION

To conclude, our experiments show that linear blasts in granular flows can be obtained in a simple setting. These blasts propagate with a velocity that can be understood using a simple model. The blasts then become unstable through a modulation of the density of the front. This instability as well as its growth rate and its wavelength can be obtained from a continuous hydrodynamic model for granular gases. These experiments allow for stringent tests of such models, which are derived from the granular kinetic theory, under extreme conditions by placing limits on the parameters entering into play. Our study also allows for a detailed exploration of the role of dissipation in the dynamics of blasts.

ACKNOWLEDGMENTS

This work benefited from a grant of the Conseil Régional d'Aquitaine.

[1] J. Bougie and K. Duckert, Phys. Rev. E **83**, 011303 (2011); J. Bougie, Sung Joon Moon, J. B. Swift, and H. L. Swinney, *ibid.* **66**, 051301 (2002).
[2] S. P. Pudasaini and C. Kröner, Phys. Rev. E **78**, 041308 (2008).
[3] P. Zamankhan, Shock Waves **17**, 337 (2008).
[4] E. C. Rericha, C. Bizon, M. D. Shattuck, and H. L. Swinney, Phys. Rev. Lett. **88**, 014302 (2002).
[5] J. F. Boudet, Y. Amarouchene, and H. Kellay, Phys. Rev. Lett. **101**, 254503 (2008).

[6] Y. Amarouchene and H. Kellay, Phys. Fluids **18**, 031707 (2006).
[7] J. F. Boudet and H. Kellay, Phys. Rev. Lett. **105**, 104501 (2010).
[8] J. F. Boudet, J. Cassagne, and H. Kellay, Phys. Rev. Lett. **103**, 224501 (2009).
[9] T. Antal, P. L. Krapivsky, and S. Redner, Phys. Rev. E **78**, 030301 (2008).
[10] G. I. Taylor, Proc. R. Soc. London A **201**, 159 (1950); **201**, 175 (1950).
[11] L. I. Sedov, J. Appl. Math.: Mech. **10**, 241 (1946).
[12] J. J. Erpenbeck, Phys. Fluids **5**, 1181 (1962).
[13] D. Ryu and E. T. Vishniac, Astrophys. J. **313**, 820 (1987).
[14] A. L. Velikovich, S. T. Zalesak, N. Metzler, and J. G. Wouchuk, Phys. Rev. E **72**, 046306 (2005).
[15] J. Grun, J. Stamper, C. Manka, J. Resnick, R. Burris, J. Crawford, and B. H. Ripin, Phys. Rev. Lett. **66**, 2738 (1991).
[16] M. J. Edwards, A. J. MacKinnon, J. Zweiback, K. Shigemori, D. Ryutov, A. M. Rubenchik, K. A. Keilty, E. Liang, B. A. Remington, and T. Ditmire, Phys. Rev. Lett. **87**, 085004 (2001).
[17] A. D. Edens *et al.*, Phys. Plasmas **17**, 112104 (2010).
[18] B. A. Remington, R. P. Drake, and D. D. Ryutov, Rev. Mod. Phys. **78**, 755 (2006).
[19] J. P. Ostriker and C. F. McKee, Rev. Mod. Phys. **60**, 1 (1988).
[20] M. I. Radulescu and N. Sirmas, arXiv:1108.3296v2 (2012).
[21] C. Cavet *et al.*, Astrophys. Space Sci. **322**, 91 (2009).
[22] E. L. Grossman, Tong Zhou, and E. Ben-Naim, Phys. Rev. E **55**, 4200 (1997).
[23] If we assume a constant thickness for the flow and the front which has a width W, conservation of matter dictates $\Phi_0 R = \Phi_1 W$ so $a = W/R$. Estimates of the width versus R give $a \sim 0.16$.